A Route for Bulk Separation of Semiconducting from Metallic Single-Wall Carbon Nanotubes

Debjit Chattopadhyay, Izabela Galeska, and Fotios Papadimitrakopoulos*

Contribution from the Nanomaterials Optoelectronics Laboratory, Department of Chemistry, Polymer Program, Institute of Materials Science, University of Connecticut, Storrs, Connecticut 06269-3136

Received September 18, 2002 ; E-mail: papadim@mail.ims.uconn.edu

Abstract: Substantial separation of single-wall carbon nanotubes (SWNTs) according to type (metallic versus semiconducting) has been achieved for HiPco and laser-ablated SWNTs. We presently argue that stable dispersions of SWNTs with octadecylamine (ODA) in tetrahydrofuran (THF) originate from the physisorption and organization of ODA along the SWNT sidewalls in addition to the originally proposed zwitterion model. Furthermore, the reported affinity of amine groups for semiconducting SWNTs, as opposed to their metallic counterparts, contributes additional stability to the physisorbed ODA. This provides a venue for the selective precipitation of metallic SWNTs upon increasing dispersion concentration, as indicated by Raman investigations.

Introduction

Single-wall carbon nanotubes (SWNTs) form a unique class of one-dimensional quantum-confined structures exhibiting either semiconducting (*sem-*) or metallic (*met-*) behavior.[1] From an electronics perspective, separation of SWNTs according to type (*met-* versus *sem-*) is of paramount importance.[1] Although *met-*SWNTs can be destructively eliminated by a current-induced oxidation,[2] this method is limited to transistor geometries and cannot be extended for bulk separation. Herein we provide the first route for the nondestructive separation of *met-* from *sem-*SWNTs for both HiPco[3] and laser-ablated[4] SWNTs. We also argue that stable dispersions of SWNTs with octadecylamine (ODA) in tetrahydrofuran (THF) originate from the physisorption and organization of ODA along the SWNT sidewalls, in addition to the originally proposed zwitterion model.[5,6]

The noncovalent functionalization of acid-treated SWNTs with ODA has been suggested to yield stable dispersions[7] by the formation of zwitterions with the carboxyl functionalities typically observed on the SWNT ends, although a few zwitterions might also be formed from sidewall defects.[5,6] Such a scenario, depicted in Chart 1A, raises serious doubts concerning the ability of these zwitterion complexes to prevent SWNT aggregation[5,6,8] in light of the fact that the van der Waals binding energy for high aspect ratio SWNTs (10^4–10^5) can be as high as 500 eV per micrometer of tube–tube contact.[9]

It has been established theoretically[10] and experimentally[11] that amines possess significant affinity for physisorption along the SWNT sidewalls. Kong and Dai[11] demonstrated drastic changes in the electrical properties of individual *sem-*SWNTs upon adsorption of linear alkylamines (chemical gating effect), wherein the electron donating power of -NH_2 groups was sufficient to cause significant change in the electrical conductance of *sem-*SWNTs. Most notably, the conductance behavior of *met-*SWNTs remained insensitive to adsorbed amines and other moieties such as NH_3 and NO_2. Consequently, the fundamental question that arises is whether ODA physisorbs and organizes along the highly curved graphitic sidewalls of SWNTs as shown in Chart 1B. Assuming that ODA organization along the graphitic sidewalls is what enables the dispersion of individual and/or bundles of SWNTs, it is conceivable that the physisorbed ODA and its organized domains experience additional stabilization on *sem-*SWNTs as opposed to their metallic counterparts. If this is the case, then the much-desired separation

* To whom correspondence should be addressed: Tel (860) 486-4347; fax (860) 486-4745.

(1) Dresselhaus, M. S.; Dresselhaus, G.; Avouris, P., Eds. *Carbon Nanotubes*: *Synthesis*, *Structure*, *Properties and Applications*, 1st ed.; Springer-Verlag: Heidelberg, Germany, 2001; Vol. 80.

(2) Collins, P. G.; Arnold, M. S.; Avouris, P. *Science* **2001**, *292*, 706−709.

(3) Nikolaev, P.; Bronikowski, M. J.; Bradley, R. K.; Rohmund, F.; Colbert, D. T.; Smith, K. A.; Smalley, R. E. *Chem. Phys. Lett.* **1999**, *313*, 91−97.

(4) Rinzler, A. G.; Liu, J.; Dai, H.; Nikolaev, P.; Huffman, C. B.; Rodriguez-Macias, F. J.; Boul, P. J.; Lu, A. H.; Heymann, D.; Colbert, D. T.; Lee, R. S.; Fischer, J. E.; Rao, A. M.; Eklund, P. C.; Smalley, R. E. *Appl. Phys. A.* **1998**, *A67*, 29−37.

(5) Hamon, M. A.; Chen, J.; Hu, H.; Chen, Y.; Itkis, M. E.; Rao, A. M.; Eklund, P. C.; Haddon, R. C. *Adv. Mater.* **1999**, *11*, 834−840.

(6) Chattopadhyay, D.; Lastella, S.; Kim, S.; Papadimitrakopoulos, F. *J. Am. Chem. Soc.* **2002**, *124*, 728−729.

(7) The term "solubilization" is frequently used to describe stable and scatter-free SWNT solutions. But the presence of both individual and small nanotube bundles has prompted us to term SWNT/ODA complexes in THF as "dispersion". However, as previously demonstrated by us[6] and another group,[9] true solutions of SWNTs can be obtained under special conditions, shown to exhibit much better resolved optical absorption spectra.

(8) Hamon, M. A.; Hu, H.; Bhowmik, P.; Niyogi, S.; Zhao, B.; Itkis, M. E.; Haddon, R. C. *Chem. Phys. Lett.* **2001**, *347*, 8−12.

(9) O'Connell, M. J.; Bachilo, S. M.; Huffman, C. B.; Moore, V. C.; Strano, M. S.; Haroz, E. H.; Rialon, K. L.; Boul, P. J.; Noon, W. H.; Kittrell, C.; Ma, J.; Hauge, R. H.; Weisman, R. B.; Smalley, R. E. *Science* **2002**, *297*, 593−596.

(10) Basiuk, E. V.; Basiuk, V. A.; Banuelos, J.-G.; Saniger-Blesa, J.-M.; Pokrovskiy, V. A.; Gromovoy, T. Y.; Mischanchuk, A. V.; Mischanchuk, B. G. *J. Phys. Chem. B* **2002**, *106*, 1588−1597.

(11) Kong, J.; Dai, H. *J. Phys. Chem. B* **2001**, *105*, 2890−2893.

Chart 1. Pictorial Representation of Possible ODA Interactions with Acid-Functionalized SWNTs through (A) Zwitterion Formation and (B) Physisorption-Assisted Organization of ODA on SWNTs Sidewalls
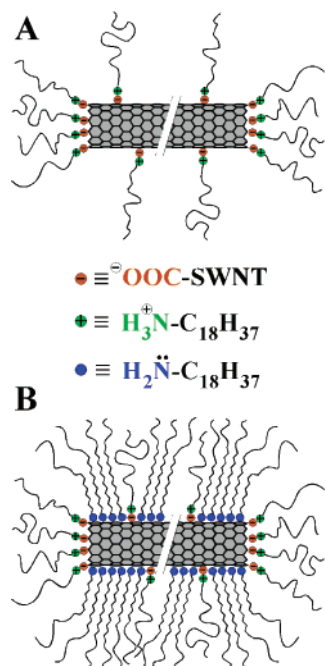
of *sem*- vs *met*-SWNTs can be envisioned by selectively destabilizing the ODA organization on *met*-SWNTs and promoting their precipitation, while their semiconducting counterparts can be retained in the supernatant.

Experimental Section

Noncovalent Functionalization of SWNTs. Laser-ablated and HiPco SWNTs were purchased from tubes@rice and Carbon Nanotechnologies. The SWNTs were carboxy-functionalized by a brief sonication-assisted oxidation in a mixture of H_2SO_4 and HNO_3 following a previously established protocol.[12,13] The noncovalent functionalization of SWNTs with octadecylamine (ODA) involves a treatment of the carboxy-terminated SWNTs in molten ODA at temperatures between 100 and 120 °C for 120 h, followed by extensive sonication-assisted washing with ethanol to remove excess ODA.[5,6] The resulting solid was finally dispersed in THF via mild sonication, followed by filtration through coarse filter paper to remove the undispersed SWNTs, with typical yields of about 75% for HiPco and less than 50% for laser-ablated SWNTs.

Raman Spectroscopy. Raman spectra from all the samples were collected with a Renishaw Ramanscope in the backscattering configuration under the same experimental conditions albeit with different laser excitations. The Stokes spectra of all the HiPco samples were obtained with the 514.5 nm (2.41 eV) and 785 nm (1.58 eV) lasers, whereas the laser-ablated SWNTs were primarily probed by the 785 nm (1.58 eV) laser in both the Stokes and the anti-Stokes regime.

Correlation between Raman Spectroscopy, SWNT Diameters, and Their Electronic Transitions. The single-wall carbon nanotube (SWNT) diameters and the electronic transitions between the density of states for *met*- and *sem*-SWNTs were calculated from the Raman

radial breathing modes (RBM). The diameters were estimated[14] by use of

$$\omega_{RBM} = (224/d) + 14$$

The transition between DOS for *met*- and *sem*-SWNTs was approximated as follows:[15]

$$^{M}E_{11} = 6\gamma_o a_{C-C}/d$$

$$^{S}E_{22} = 4\gamma_o a_{C-C}/d$$

$$^{S}E_{33} = 8\gamma_o a_{C-C}/d$$

where $^{M}E_{11}$, $^{S}E_{22}$, and $^{S}E_{33}$ indicate transitions between the first, second, and third pair of singularities of *met*- ($^{M}E_{11}$) and *sem*-SWNTs ($^{S}E_{22}$ and $^{S}E_{33}$), respectively; ω_{RBM} is the RBM frequency (in reciprocal centimeters), d is the diameter (in nanometers), γ_o is the overlap integral (2.9 ± 0.5 eV), and a_{C-C} is the carbon–carbon bond length (0.144 nm).

Additionally, the energy of the scattered beam is at $E_{laser} - E_{phonon}$ for the Stokes and $E_{laser} + E_{phonon}$ for the anti-Stokes processes, with $E_{phonon} \cong 0.197$ eV.[16]

Prior to the collection of Raman spectra from either the free-standing or the drop-cast SWNT films, all the samples were vacuum-dried (less than 1 Torr) at 200 °C, necessary to suppress the background fluorescence associated with ODA, which further eliminates any possible distortions to the electronic band structure of semiconducting SWNTs from the electron-donating effect of ODA.

Differential Scanning Calorimetry. DSC scans were performed on a Perkin-Elmer DSC 7. SWNT/ODA samples were obtained by drop-casting and careful drying of their THF dispersions. Careful attention was paid to the removal of excess ODA from the SWNT/ODA complexes prior to their dispersion in THF, by repeated sonication-assisted washing in ethanol. DSC scans of neat ODA was obtained from as-supplied ODA without further purification.

Thermogravimetric Analysis. TGA analysis on neat ODA and SWNT/ODA aliquots was performed on a Perkin-Elmer-TGA7, at a scan rate of 5 °C/min under a nitrogen atmosphere.

Accelerated Precipitation of *met*- from *sem*-SWNTs. This was achieved by immersing the ODA/SWNTs/THF dispersion in a preheated water bath (60 °C) at ambient pressure, required for speedier solvent evaporation.

Four-Point Probe Conductivity Measurements. Samples of comparable thickness were fabricated by filtration, following which free-standing films were peeled and vacuum annealed (at less than 1 mTorr) at 420 °C for 20 h to eliminate ODA. Conductivity measurements were performed on a custom-built apparatus equipped with a current and high-input impedance voltmeter, at low current levels (9 mA) so as to prevent sample overheating. The conductivity values were calculated from the empirical equation ($\rho = 2\pi SV/I$), where S is the probe spacing (assumed to be identical for all probes; 0.025 cm in our case), I is the current supplied by a constant source, and V is the voltage measured by a high-input impedance voltmeter.

Results and Discussion

To validate the hypothesis of selective precipitation of *met*-SWNT/ODA complexes, acid-treated HiPco[3] [with diameter (d) distribution between 0.8 and 1.3 nm and d_{avg} ca. 1 nm][17] and laser-ablated (with diameter distribution between 1.15 and 1.55

(12) Liu, J.; Rinzler, A. G.; Dai, H.; Hafner, J. H.; Bradley, R. K.; Boul, P. J.; Lu, A.; Iverson, T.; Shelimov, K.; Huffman, C. B.; Rodriguez-Macias, F. J.; Shon, Y.-S.; Lee, T. R.; Colbert, D. T.; Smalley, R. E. *Science* **1998**, *280*, 1253–1256.
(13) Chattopadhyay, D.; Galeska, I.; Papadimitrakopoulos, F. *Carbon* **2002**, *60*, 960–965.
(14) Rao, A. M.; Chen, J.; Richter, E.; Schlecht, U.; Eklund, P. C.; Haddon, R. C.; Venkateswaran, U. D.; Kwon, Y. K.; Tomanek, D. *Phys. Rev. Lett.* **2001**, *86*, 3895–3898.
(15) White, C. T.; Mintmire, J. W. *Phys. Rev. Lett.* **1998**, *81*, 2506–2509.
(16) Brown, S. D. M.; Corio, P.; Marucci, A.; Dresselhaus, M. S.; Pimenta, M. A.; Kneipp, K. *Phys. Rev. B* **2000**, *61*, R5137–R5140.

nm and d_{avg} ca. 1.37 nm) SWNTs[4] were dispersed in THF by the previously established zwitterion route.[5,6] As will become apparent later in the discussion, both *met*- and *sem*-SWNTs can be dispersed by this treatment, yielding a transparent, heavily colored solution stable at concentrations between 1 and 0.1 mg/mL. To obtain such SWNT/ODA dispersions in THF, temperatures in excess of 90 °C are required during the treatment of acid-functionalized SWNTs with ODA.[5,6] Although the melting point of ODA is ca. 58 °C, differential scanning calorimetry (DSC) and cross-polar optical microscopy indicate the presence of a higher melting endotherm at ca. 87 °C that is tentatively assigned to a mesophase-isotropic transition (Figure S1, Supporting Information). The temperature-sensitive ODA functionalization closely resembles the high-temperature (above melting point) solubilization of the structurally regular and chemically inert polyhydrocarbons, such as linear high-density polyethylene and isotactic polypropylene.[18] Moreover, the amphiphilic character of ODA is known to promote self-organization on interfaces, melts, and polar solvents,[19] to form mono- and multilayer films in a Langmuir−Blodgett fashion[20] and to exhibit liquid crystalline behavior when complexed with metals[21] or associated with polymers.[22] The possibility that ODA behaves much like *n*-hexadecylamine (HDA) (homologous alkylamine, with two fewer carbon atoms than ODA) that was shown to organize on, passivate, and solubilize CdSe quantum dots[23] prompted us to quantify the amount of ODA that remains physisorbed on SWNTs after extensive washing with ethanol. Thermogravimetric analysis indicated a significant weight loss (more than 90%, Figure S3, Supporting Information) between 150 and 300 °C, which is in agreement with the substantial amount of physisorbed ODA, as depicted in Chart 1B. Furthermore, DSC data for both HiPco and laser-ablated SWNTs/ODA complexes indicate the presence of both sharp and broad endothermic (melting) transitions as shown in Figure S2 in the Supporting Information. These have been associated with melting of SWNT-associated ODA domains exhibiting various degrees of crystal perfection. Although the majority of the endothermic transitions occur below the melting point of pure ODA (i.e., 58 °C), the presence of higher endotherms might be indicative of ODA crystallized in tilted arrays, similar to those reported for CdSe/HDA quantum dot systems.[23]

Following an interesting observation of the gradual sedimentation of parts of the ODA-dispersed SWNTs after being left undisturbed over a period of few weeks, as will become apparent later on in the discussion, a careful analysis of that precipitate and supernatant provided some remarkable differences in terms of the type of SWNTs present in each component. If our dispersion hypothesis is valid, then *met*-SWNTs should be the dominant constituent of the precipitate. The sedimentation process can be accelerated (to minutes instead of months) by

solvent evaporation, which increases the local concentration of the dispersed SWNTs and promotes greater interactions between nanotubes. However, on the basis of the presence of small bundles (composed of 2−6 nanotubes)[24] along with individual ODA-encased SWNTs, both the supernatant and the precipitate are expected to have a finite component of *met*- and *sem*-SWNTs, respectively. As elaborated below, this is expected to be more relevant for laser-ablated SWNTs, wherein their narrow diameter distribution promotes better packing in the hexagonal close-packed rope lattice.

In this study, the Raman spectra of four samples designated as-supplied (**I**), dispersed before precipitation (**II**), supernatant (**III**), and precipitate (**IV**) were collected from free-standing (**I**, **IV**) or drop-casted (**II**, **III**) films on quartz substrates with thickness exceeding 1 μm. The strong coupling between electrons and photons, arising from the 1D confinement-induced van Hove singularities in the density of states (DOS) for SWNTs, gives rise to highly unusual diameter-dependent resonance Raman spectra, reflected by the radial breathing mode (RBM) profiles[25] (ca. 100−300 cm^{-1} for SWNTs in the present study). Resonance conditions apply when the energy of the incident and/or the scattered photon matches an interband electronic transition of the SWNTs and is typically within ±0.1 eV of the laser excitation energy (E_{laser}).[25] Additionally, the distinct differences in the line shape of the tangential G-band (ca. 1500−1605 cm^{-1}) provide a simple method for distinguishing between *met*- and *sem*- SWNTs.[26] Typically, the G-band for *sem*-SWNTs has two distinct Lorentzian peaks (ca. 1592 and 1567 cm^{-1}) with relatively narrow line widths. The peak at ca. 1592 cm^{-1} is associated with vibrations along the SWNT axis (ω^+_G), while the peak at ca. 1567 cm^{-1} has been attributed to vibrations along the tangential direction (ω^-_G). Although the ω^+_G component of *met*-SWNTs has a Lorentzian line shape that is almost as narrow as that for *sem*-SWNTs, the ω^-_G constituent is broad and best described by a Breit−Wigner−Fano (BWF) line shape.[27]

Figure 1 provides a color-coded illustration of the anticipated diameter-dependent resonance for HiPco (**A**) and laser-ablated (**B**) SWNTs, for both types, *met*- and *sem*-, upon excitation with the 514.5 nm (2.41 eV) and the 785 nm (1.58 eV) lasers, depicted in green and red, respectively. As indicated in Figure 1A, for HiPco the 2.41 eV excitation mostly probes *met*-SWNTs and very few *sem*-SWNTs arising from the E_{laser} overlap with $^SE_{33}$ transitions for larger diameter (1.27−1.15 nm) *sem*-SWNTs. If our proposed hypothesis is correct, the RBM profile of **IV** should be similar to that of **I**, whereas that for the SWNTs remaining in the supernatant **III** should be dramatically different. This is amply demonstrated by the insets in Figure 2A (bottom inset), wherein a strong correlation exists between the resonant diameters for **IV** and **I** as opposed to that of **III**, which exhibits a single broad peak at ca. 190 cm^{-1} ($d \cong 1.27$ nm). A comparison of the G-bands for all four samples in Figure 2A

(17) Zhou, W.; Ooi, Y. H.; Russo, R.; Papanek, P.; Luzzi, D. E.; Fischer, J. E.; Bronikowski, M. J.; Willis, P. A.; Smalley, R. E. *Chem. Phys. Lett.* **2001**, *350*, 6−14.

(18) Beach, D. L.; Kissin, Y. V. In *Encyclopedia of polymer science and engineering*, 2nd ed.; Mark, H. F., Bikales, N. M., Overberger, C. G., Menges, F., Eds.; Wiley: New York, 1986; Vol. 6, pp 454−490.

(19) Piculell, L.; Thuresson, K.; Lindman, B. *Polym. Adv. Technol.* **2001**, *12*, 44−69.

(20) Lee, Y.-L. *Langmuir* **1999**, *15*, 1796−1801.

(21) Paleos, C. M.; Margomenou-Leonidopoulou, G.; Anastassopoulou, J. D.; Papaconstantinou, E. *Mol. Cryst. Liq. Cryst.* **1988**, *161*, 373−383.

(22) Paleos, C. M.; Tsiourvas, D.; Anastassopoulou, J.; Theophanides, T. *Polymer* **1992**, *33*, 4047−4051.

(23) Meulenberg, R. W.; Strouse, G. F. *J. Phys. Chem. B* **2001**, *105*, 7438−7445.

(24) Chen, J.; Rao, A. M.; Lyuksyutov, S.; Itkis, M. E.; Hamon, M. A.; Hu, H.; Cohn, R. W.; Eklund, P. C.; Colbert, D. T.; Smalley, R. E.; Haddon, R. C. *J. Phys. Chem. B* **2001**, *105*, 2525−2528.

(25) Rao, A. M.; Richter, E.; Bandow, S.; Chase, B.; Eklund, P. C.; Williams, K. A.; Fang, S.; Subbaswamy, K. R.; Menon, M.; Thess, A.; Smalley, R. E.; Dresselhaus, G.; Dresselhaus, M. S. *Science* **1997**, *275*, 187−191.

(26) Pimenta, M. A.; Marucci, A.; Empedocles, S. A.; Bawendi, M. G.; Hanlon, E. B.; Rao, A. M.; Eklund, P. C.; Smalley, R. E.; Dresselhaus, G.; Dresselhaus, M. S. *Phys. Rev. B* **1998**, *58*, R16016−R16019.

(27) Brown, S. D. M.; Jorio, A.; Corio, P.; Dresselhaus, M. S.; Dresselhaus, G.; Saito, R.; Kneipp, K. *Phys. Rev. B* **2001**, *63*, 15414−15422.

ω_{RBM} (cm^{-1})	Diameter d (nm)	$^{M}E_{11}$ (eV)	$^{S}E_{22}$ (eV)	$^{S}E_{33}$ (eV)
190.0	1.27	1.97	1.31	2.62
201.0	1.20	2.09	1.39	2.79
204.7	1.17	2.13	1.42	2.84
205.9	1.16	2.15	1.43	2.86
210.0	1.14	2.19	1.46	2.92
214.7	1.12	2.24	1.50	2.99
215.7	1.11	2.26	1.50	3.01
226.2	1.06	2.37	1.58	3.16
227.2	1.05	2.39	1.59	3.18
233.3	1.02	2.45	1.64	3.27
235.0	1.01	2.47	1.65	3.30
246.1	0.97	2.60	1.73	3.46
266.4	0.89	2.82	1.88	3.76
267.8	0.88	2.84	1.89	3.79
271.3	0.87	2.88	1.92	3.84
158.3	1.55	1.61	1.08	2.15
160.0	1.53	1.63	1.09	2.18
167.0	1.46	1.71	1.14	2.28
174.2	1.40	1.79	1.19	2.39
176.7	1.38	1.82	1.21	2.43
177.3	1.37	1.83	1.22	2.44
184.8	1.31	1.91	1.27	2.55
201.0	1.20	2.09	1.39	2.79
204.7	1.17	2.13	1.42	2.84
205.9	1.16	2.15	1.43	2.86
208.0	1.15	2.17	1.45	2.89

A HiPco

B Laser Ablated

Figure 1. Calculated diameters and electronic transitions for *met-* and *sem-*SWNTs from the Raman radial breathing modes (ω_{RBM}) for (A) HiPco and (B) laser-ablated SWNTs, where $^{M}E_{11}$, $^{S}E_{22}$, and $^{S}E_{33}$ indicate transitions between the first, second, and third pair of singularities of *met-* ($^{M}E_{11}$) and *sem-*SWNTs ($^{S}E_{22}$ and $^{S}E_{33}$), respectively. The colors indicate the transitions from the corresponding diameter SWNTs anticipated to be in resonance with the 2.41 eV (green) and 1.58 eV (red) laser excitation (darker shades approximate the maximum expected resonances).

provides an additional qualitative insight into the type of SWNTs (i.e., *met-* vs *sem-*). As previously alluded to, the dispersed before precipitation sample **II** contains both *met-* and *sem-*SWNTs, evidenced not only by the broad shoulder at ca. 1530 cm^{-1} (marked with star) but also by its RBM profile (top inset in Figure 2A) showing features at ca. 247 and 267 cm^{-1} that are also prominent in **IV** and **I**. However, the disappearance of all these RBM peaks in **III** points to the elimination of *met-*SWNTs during precipitation. Additionally, the sharp ω^{+}_{G} (ca. 1592 cm^{-1}) and ω^{-}_{G} (ca. 1567 cm^{-1}) peaks of **III** are characteristic of *sem-*SWNTs, as opposed to **I**, **II**, and **IV**, and indicate the substantial separation of *sem-*SWNTs from its metallic counterparts. This argument is further supported by the G-bands for **IV** and **I** that have the typical BWF line shapes attributed to *met-*SWNTs. Moreover, the much broader ω^{-}_{G} component of **IV** (centered ca. 1520 cm^{-1}) not only reflects the smaller d_{avg} in HiPco[26] but also provides additional confirmation that the precipitate is indeed enriched with *met-*SWNTs. Typically, the ω^{+}_{G} component in *met-*SWNTs shows only a weak frequency dependence on nanotube diameter and appears around 1580 cm^{-1}.[26] The substantial presence of *sem-*SWNTs in **I** compared to **IV** also concurs with the observed G-band frequency shift from 1591 to 1585 cm^{-1}.

As illustrated in Figure 1A, the 1.58 eV laser selectively probes only *sem-*SWNTs in HiPco (red area, $^{S}E_{22}$ column), allowing us to not only validate the separation process but also interrogate its selectivity in enriching the supernatant with *sem-*

SWNTs. This is best demonstrated in Figure 2B, where the RBM profile for **IV** is almost absent when compared to either **I** or **III,** necessitating scaling ×10 to enhance visualization of these features. This lends further credence to the fact that *sem-*SWNTs are preferentially retained in the supernatant. The peak at ca. 267 cm^{-1} ($d \cong 0.88$ nm) emerges as the dominant feature of **III** (stronger than its G-band), which might be associated with either larger Raman cross-sectional areas[28] or higher solubility[29] for smaller diameter SWNTs. These findings point to a substantial separation of *met-* from *sem-*SWNTs in HiPco, wherein most of the *sem-*SWNTs can be retained in the supernatant while a majority of the *met-*SWNTs can be selectively extracted in the precipitate.

To further demonstrate the viability of the concept, laser-ablated SWNTs were subjected to the similar dispersion—precipitation process used for HiPco. However, the relatively narrow 1.37 ± 0.18 nm diameter distribution of laser-ablated SWNTs provides very few small-diameter (less than 1.2 nm) *met-*SWNTs that can be probed by the 2.41 eV laser. For this, the 1.58 eV excitation was utilized in both the Stokes ($E_{laser} - E_{phonon} \cong 1.38$ eV) and the anti-Stokes ($E_{laser} + E_{phonon} \cong 1.78$ eV) regimes to probe *sem-*SWNTs with diameters smaller than 1.2 nm and *met-*SWNTs with diameters larger than 1.4 nm, respectively. Typically, in the anti-Stokes Raman spectra an additional enhancement of the vibrational features for *met-*SWNTs has been observed experimentally relative to *sem-*SWNTs on account of their stronger electron—phonon coupling.[16]

Figure 3 depicts the anti-Stokes spectra of **I**−**IV** for the laser-ablated SWNTs, while the Stokes spectrum is shown in Figure 4. As anticipated, the broad BWF line shape typical for *met-*SWNTs is evident in the anti-Stokes spectra of **IV** and **I**, while that for **II** appears to be significantly subdued by at least a factor of 5 as shown in the ×5 inset, appended for spectral clarity. Interestingly, in **IV** the G-band has a more pronounced BWF line shape, with a dominant ω^{-}_{G} component centered at ca. −1530 cm^{-1},[26] pointing to enrichment of the precipitate with *met-*SWNTs. A comparison of the RBM profiles for **I** and **II** indicates qualitative similarities, with the −208 and −167 cm^{-1} peaks as their most prominent features. The RBM peak at −167 cm^{-1} can be attributed to *met-*SWNTs ($d \cong 1.46$ nm, $^{M}E_{11} \cong 1.71$ eV) while the feature at −208 cm^{-1} corresponds to *sem-*SWNTs ($d \cong 1.15$ nm, $^{S}E_{22} \cong 1.45$ eV).

Interestingly, in the spectrum for **IV** the contribution from the −208 cm^{-1} component is substantially reduced, pointing to an enrichment of the precipitate with *met-*SWNTs that is in accordance with the line shape changes of the G-band. This complements the spectrum for **III**, where a comparable decrease in intensity of the −167 cm^{-1} peak is evident, with the peak at −208 cm^{-1} now appearing as the dominant component, indicating that *sem-*SWNT are retained in the supernatant, which corroborates the single sharp peak at 210 cm^{-1} in its Stokes spectra (Figure 4).

As opposed to HiPco, laser−ablated SWNTs exhibit larger metallic (ω_{RBM} at −167 cm^{-1}) and semiconducting (ω_{RBM} at −208 cm^{-1}) residues in **III** and **IV**, respectively. This may originate from the more uniform diameter distribution of laser-

(28) Dresselhaus, M. S.; Eklund, P. C. *Adv. Phys.* **2000**, *49*, 705−814.
(29) Bahr, J. L.; Yang, J.; Kosynkin, D. V.; Bronikowski, M. J.; Smalley, R. E.; Tour, J. M. *J. Am. Chem. Soc.* **2001**, *123*, 6536−6542.
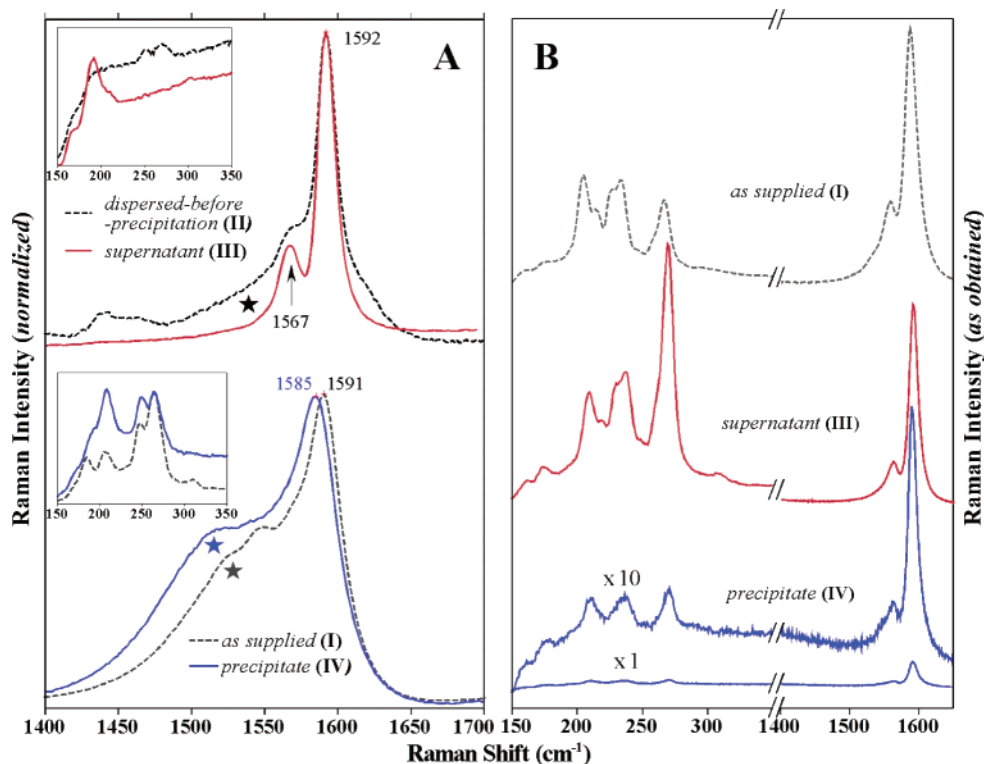
Figure 2. Stokes spectra for HiPco SWNTs obtained with (A) 2.41 eV and (B) 1.58 eV laser. The stars indicate the locations of the ω^-_G (BWF) component for *met*-SWNTs.
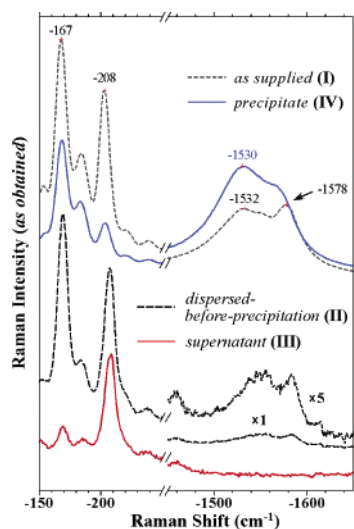

Figure 3. Anti-Stokes spectra for laser-ablated SWNTs obtained with the 1.58 eV laser.

Figure 4. Stokes spectra for laser-ablated SWNTs obtained with the 785 nm (1.58 eV) laser excitation.

ablated SWNTs, which is known to promote more ordered rope lattices[4,17] and can lead to enhanced bundling in THF dispersions.[5,6] Further studies to quantify the extent of separation for HiPco and laser-ablated SWNTs are currently underway, involving determination of precise diameter distribution and correlation to Raman intensities.

Additionally, four-point probe conductivity measurements on free-standing HiPco SWNTs films were performed to provide further proof of the separation. Free-standing films of metallic-(**III**) and semiconducting- (**IV**) enriched HiPco SWNTs were fabricated by filtration followed by vacuum annealing to eliminate ODA and to allow the separated SWNT to form percolated structures with reproducible conductivity values. The
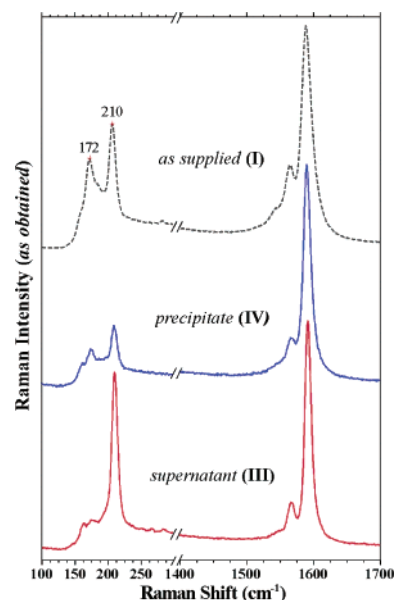
conductivity of these samples was compared to the as-supplied HiPco SWNTs (10% metal content), and the corresponding acid-treated sample (with catalyst content <0.5 wt %), upon which the separation was performed. SWNTs were annealed under the same condition as the other free-standing films. As expected, the effect of metallic impurities is manifested in the conductivity of the as-supplied HiPco SWNTs (conductivity 15.60 S/cm), which is 30 times more conductive than the acid-purified and annealed sample (conductivity 0.51 S/cm). Compared to this, the conductivity of the metallic-enriched and annealed SWNT fraction (**III**) is 0.78 S/cm, which is 4.5 times greater than that

of the semiconducting-enriched and annealed SWNT fraction (**IV**, 0.17 S/cm). These results are in qualitative agreement with the Raman data inferred from Figure 2 that clearly demonstrate the viability of our separation methodology.

Conclusions

To the best of our knowledge, this represents the first methodology for the bulk enrichment of SWNTs, wherein *sem*-SWNT can be retained in the supernatant as a result of a stronger ODA physisorption on their sidewalls as opposed to *met*-SWNTs. We believe that comprehensive understanding of all the parameters involved, such as the degree of bundling in the THF dispersions and effects of temperature and concentration fluctuations during precipitation, as well as successive precipitation−redispersion cycles, could eventually lead to a far greater degree of separation. This will have significant ramifications for a wide range of SWNT applications such as nanoelectronics, sensors, actuators, field emission devices, etc., where the use of either semiconducting or metallic nanotubes can be tailored as needed.

Supporting Information Available: Figures S1, S2, and S3 as described in the text (PDF). This material is available free of charge via Internet at http://pubs.acs.org.

JA028599L